International Journal of Energy Research

INTERNATIONAL JOURNAL OF ENERGY RESEARCH
Int. J. Energy Res. 2013; **37**:310–322
Published online 23 September 2011 in Wiley Online Library (wileyonlinelibrary.com). DOI: 10.1002/er.1910

Chimney shape numerical study for solar chimney power generating systems

Tingzhen Ming[1,*,†], Renaud Kiesgen de Richter[2], Fanlong Meng[1], Yuan Pan[3] and Wei Liu[1]

[1]School of Energy and Power Engineering, Huazhong University of Science and Technology, Wuhan, China
[2]Tour-Solaire.Fr, 8 Impasse des Papillons, F34090 Montpellier, France
[3]College of Electrical and Electronic Engineering, Huazhong University of Science and Technology, Wuhan, China

SUMMARY

A large number of researchers have paid great attention to solar chimney (SC) power generating technology, but only a few have studied the chimney configuration. Taking a 10 MW SC system as an example, the physical and mathematical models illustrating the fluid flow, heat transfer and output power features of the system are established. Based on constraints such as equal chimney bottom section area or equal chimney surface area, the impact of several sizes of three different chimney configurations upon the chimney outlet air temperature and velocity, system output power and efficiency is analyzed and the influence of the height-to-diameter ratio (H/D) of the cylindrical chimney on system performance is studied as well. After a comprehensive analysis of system output power and efficiency, it is proved by the numerical simulation that the cylindrical chimney would be the best choice among the three basic configurations, whose optimum H/D value ranges from 6 to 8. Copyright © 2011 John Wiley & Sons, Ltd.

KEY WORDS

solar chimney; output power; efficiency; chimney; collector; turbine

Correspondence

*Tingzhen Ming, School of Energy and Power Engineering, Huazhong University of Science and Technology, Wuhan, China.
†E-mail: mtzhen@163.com

Received 12 April 2011; Revised 14 June 2011; Accepted 9 July 2011

1. INTRODUCTION

Issues of energy security and environmental protection have been featured prominently in China recently and if not effectively addressed, they will severely impede China's economic development. During the 2009 Copenhagen Climatic Change Conference, the Chinese government announced the goal of controlling greenhouse gas emission, by 2020, to reduce the carbon dioxide emission per unit of the gross domestic product from 40% to 45% compared with 2005's figures [1]. It is, therefore, necessary for us to push forward the development of the renewable energy power generating technologies, which are of great importance if China is to meet the emissions reduction goal.

The solar chimney (SC) is an energy-saving and environmentally friendly renewable energy power generating technology compared with existing coal-fired power stations, featuring continuous power generating and low operation costs in contrast with other current renewable energy power generating technologies [2,3]. For Weinrebe [4], in 1999, the greenhouse gas emissions calculated in CO_2 equivalents (g/KWh) form a 200 MW SC, almost similar as for wind turbine or a dish Stirling, almost four times lower than for photovoltaics, and more than 50 times less than for an Australian coal plant (respectively, 18, 16, 21, 84 and 980 g/KWh). Meanwhile, for Bernardes [5], the ecological analysis results in approximately 170 and 70 g CO_2-equivalents/kWh, respectively, for 5 MW SC and 100 MW SC. The consumption of exhausting energetic and mineral resources as well as specific CO_2 decreases with larger plants. This also depends on the life expectancy taken for the SC which can be up to more than 100 years. Moreover, it wastes no water resources as it does not need any heat sink and could help improve the surrounding environment as well as rebuild local ecosystems. Suitable to be adopted in arid and semi-arid areas as well as developing countries where solar insolation is abundant, it implies a wide field of applications with good prospects [6].

Many researchers have carried out studies on SC for several decades. In the beginning, the main focus was on the influence on system power generating performance based on thermodynamic analysis [7–9]. Later, in order to conduct costs pre-estimation on large-scale SC system, the research group led by Prof. Sherif [10–12] established mathematical models and experimental devices

describing the fluid flow and heat transfer features of the experimental systems while von Backström *et al*. [13,14] put emphasis on turbine performance of the SC system. Furthermore, steady state numerical simulations of fluid flow and heat transfer based on a two-dimensional SC model were performed by Pastohr *et al*. [15]. Recently, Maia *et al*. [16] evaluated the influence of some parameters on the behaviour of the airflow in a solar chimney (SC) and showed that the height and diameter of the chimney are the most important physical variables. As well, Bonnelle *et al*. [17] optimized the height-to-diameter ratio (H/D) ratio from the trade-off between, on the one hand, the cost which is a function, not necessarily proportional, of the surface of the envelope, and on the other hand, of the fluid mechanics losses (turbulent losses and loss of the dynamic pressure at the top of the stack), which are both roughly proportional to the kinetic energy. Their conclusions are that these losses are strongly deterrent against too thin chimneys, but are quite negligible for large diameters.

Ming *et al*. [18] set up an analytical model of a system driving mechanism and carried out calculation to show the influence of system relative pressure and driving force on the output power and efficiency, followed by a detailed study on power storage features of the SC system [19–21]. The dependence of the work potential on the air flowing into the air collector from the heat gained inside the collector, air humidity and atmospheric pressure as a function of elevation has been studied by Ninic [22]. As the air flux is very important and as the chimneys are located in warm and dry deserts, humidity is low, the air is never saturated at any height inside of the SC towers envisioned in this paper and the temperature and pressure conditions inside the chimney never reach the dew point. However, several publications have studied the cloud formation in the plumes of SC [23–25].

In fact, some researches also concentrated on shapes and configurations of the SC's chimney, where researchers hold contradictory opinions. In numerical calculation and theoretical analysis, Schlaich *et al*. [6] chose the cylindrical chimney, with von Backström [13,14] and Pasumarthi *et al*. [10,11] using the divergent chimney and conical chimney respectively.

In this paper, based on a 10 MW SC, we developed the mathematical models to describe the fluid flow, heat transfer and output power features of the SC system mainly consisting of energy storage layer, collector, turbine and chimney and put more emphasis on chimney configuration's influence on SC system performance. However, the analysis of the chimney strength and resistance to wind load or to earthquakes, are not in the scope of this paper. The use of a double curvature surface is known for structure strengthening, and quite often, the cooling towers have hyperbolical shells, and chimneys are usually reinforced by stiffening rings [26–28]. In addition, the outside cross wind influence on the air discharge from the top of the chimney is a very important effect; related research work can be found in reference [29,30].

2. PHYSICAL AND MATHEMATICAL MODEL

2.1. Physical model

At first, we set up axisymmetric physical models of 10 MW SCs (with basic parameters as shown in Table I) based on two-dimensional assumptions. Taking Case 1 in Table I as an example, the collector is 1000 m in radius, and its height varies from 2.5 m at its periphery to 10 m in the center. The chimney is 800 m high, and its diameter is 80 m at its base. From its base to the top, the chimney diameters vary linearly, i.e. D_t=40 m means chimney diameters decrease from 80 m at the base to 40 m at the top. In the physical model, the collector canopy is made of transparent glass, and the bottom porous soil bed serves as the energy storage layer. In order to reduce the heat loss, the collector and the chimney are smoothly connected. Besides this, a simplified turbine model based on two-dimensional assumptions is placed at the chimney bottom. The energy storage layer is 5 m thick.

2.2. Mathematical model

The system performance of a SC depends on the system dimensions and the ambient conditions. The former mainly includes the chimney height and radius and collector radius, while the latter includes the solar radiation, ambient temperature and wind velocity. The analysis described in this paper is based on the following simplifying assumptions:

1. Axisymmetric flow of the air in the collector, i.e. non-uniform heating of the collector surface in terms of the sun's altitude angle is neglected.
2. Air flow inside the collector and the chimney can be regarded as incompressible flow, and Boussinesq hypothesis is applicable in this system.
3. The collector is placed over a plain surface. There is a slope from the inlet to the center of the collector canopy, but it can be negligible considering its large collector radius.
4. An average value for the optical properties of a certain material is considered to estimate the global solar radiation incident on the absorber surface. In the meantime, for a certain global solar radiation, air flow and heat transfer of the system are regarded as steady state.

Table I. Parameters for basic dimensions of the 10 MW SCs.

	Collector		Chimney	
Case	Radius	Height	Height	Diameter configuration
1	1000 m	2.5–10 m	800 m	D_b=80 m, D_t=40–120 m
2	1000 m	2.5–10 m	800 m	D_b=100–60 m, D_t=60–100 m
3	1500 m	2.5–12 m	600 m	D_b=D_t=60–160 m

The numerical simulation was processed by software Fluent 6.3.26, adopting the finite volume method for the solution of the differential equations, the standard $k-\varepsilon$ equation model as the turbulent flow model, standard wall function method in wall treatment SIMPLEC algorithm in pressure and velocity decoupling, the QUICK form in formulating momentum equations and energy equations.

The fluid within the collector and the chimney flows vigorously and turbulently. The axisymmetric forms of corresponding continuous equation, Navier–Stokes equation, energy equation and turbulent flow equation based on two-dimensional assumptions are as follows:

$$\frac{\partial u}{\partial x}+\frac{1}{r}\frac{\partial (rv)}{\partial r}=0 \tag{1}$$

$$\rho\left(\frac{\partial (uu)}{\partial x}+\frac{1}{r}\frac{\partial (rvu)}{\partial r}\right)=-\frac{\partial p}{\partial x}+\frac{\partial}{\partial x}\left((\mu+\mu_t)\frac{\partial u}{\partial x}\right)+\frac{1}{r}\frac{\partial}{\partial r}\left((\mu+\mu_t)r\frac{\partial u}{\partial r}\right) \tag{2}$$

$$\rho\left(\frac{\partial (uv)}{\partial x}+\frac{1}{r}\frac{\partial (rvv)}{\partial r}\right)=\frac{\partial}{\partial x}\left((\mu+\mu_t)\frac{\partial v}{\partial x}\right)+\frac{1}{r}\frac{\partial}{\partial r}\left((\mu+\mu_t)r\frac{\partial v}{\partial r}\right) \tag{3}$$

$$\rho\left(\frac{\partial (uT)}{\partial x}+\frac{1}{r}\frac{\partial (rvT)}{\partial r}\right)=\frac{\partial}{\partial x}\left(\left(\frac{\mu}{\mathrm{Pr}}+\frac{\mu_t}{\sigma_T}\right)\frac{\partial T}{\partial x}\right)+\frac{1}{r}\frac{\partial}{\partial r}\left(r\left(\frac{\mu}{\mathrm{Pr}}+\frac{\mu_t}{\sigma_T}\right)\frac{\partial T}{\partial r}\right) \tag{4}$$

$$\rho\left(\frac{\partial (\kappa u)}{\partial x}+\frac{1}{r}\frac{\partial (rv\kappa)}{\partial r}\right)=\frac{\partial}{\partial x}\left(\left(\mu+\frac{\mu_t}{\sigma_\kappa}\right)\frac{\partial \kappa}{\partial x}\right)+\frac{1}{r}\frac{\partial}{\partial r}\left(\left(\mu+\frac{\mu_t}{\sigma_\kappa}\right)r\frac{\partial \kappa}{\partial r}\right)+G_\kappa-\rho\varepsilon \tag{5}$$

$$\rho\left(\frac{\partial (\varepsilon u)}{\partial x}+\frac{1}{r}\frac{\partial (rv\varepsilon)}{\partial r}\right)=\frac{\partial}{\partial x}\left(\left(\mu+\frac{\mu_t}{\sigma_\varepsilon}\right)\frac{\partial \varepsilon}{\partial x}\right)+\frac{1}{r}\frac{\partial}{\partial r}\left(\left(\mu+\frac{\mu_t}{\sigma_\varepsilon}\right)r\frac{\partial \varepsilon}{\partial r}\right)+\frac{\varepsilon}{\kappa}(c_1G_\kappa-c_2\rho\varepsilon) \tag{6}$$

where, G_k is a production item of turbulent flow kinetic energy caused by average velocity grade and $G_k=-\rho\widetilde{u'_iu'_j}\frac{\partial u_j}{\partial x_i}$; G_b is a production item of turbulent flow kinetic energy caused by the uplift; σ_k and σ_ε are constants in the $k-\varepsilon$ equation; $\beta$is the volume expansion coefficient and $\beta\approx 1/T$.

Air flow within the energy storage layer, the collector and the chimney are interrelated. Therefore, when the heat transfer and fluid flow features of the air inside the energy storage layer are studied, air flow within the other two parts should be taken into consideration as well. As the energy storage layer is made of materials such as soil, gravel sand, etc., which could be seen as porous medium, the air normally flows slowly compared with that inside the chimney and the collector. The Brinkman–Forchheimer extended Darcy model is about to be employed in numerical simulation [31].

$$\frac{\partial u}{\partial x}+\frac{1}{r}\frac{\partial (rv)}{\partial r}=0 \tag{7}$$

$$\frac{\rho}{\varphi^2}\left(\frac{\partial (uu)}{\partial x}+\frac{1}{r}\frac{\partial (rvu)}{\partial r}\right)=-\frac{\partial p}{\partial x}+\frac{\partial}{\partial x}\left(\mu_m\frac{\partial u}{\partial x}\right)+\frac{1}{r}\frac{\partial}{\partial r}\left(r\mu_m\frac{\partial u}{\partial r}\right)-\frac{\mu u}{K}-\frac{\rho F}{\sqrt{K}}\sqrt{u^2+v^2}u+\rho g\beta(T-T_e) \tag{8}$$

$$\frac{\rho}{\varphi^2}\left(\frac{\partial (uv)}{\partial x}+\frac{1}{r}\frac{\partial (rvv)}{\partial r}\right)=\frac{\partial}{\partial x}\left(\mu_m\frac{\partial v}{\partial x}\right)+\frac{1}{r}\frac{\partial}{\partial r}\left(r\mu_m\frac{\partial v}{\partial r}\right)-\mu_m\frac{v}{r^2}-\frac{\mu u}{K}-\frac{\rho F}{\sqrt{K}}\sqrt{u^2+v^2}v \tag{9}$$

$$\rho_m c_{p,m}\left(\frac{\partial (uT)}{\partial x}+\frac{1}{r}\frac{\partial (rvT)}{\partial r}\right)=\frac{\partial}{\partial z}\left(\lambda_m\frac{\partial T}{\partial x}\right)+\frac{1}{r}\frac{\partial}{\partial r}\left(r\lambda_m\frac{\partial T}{\partial r}\right) \tag{10}$$

where, u_d、v_d represent Darcy velocity within the energy storage layer; φ、μ_m、λ_m、λ_s and λ_a are porosity, surface heat conduction coefficient and effective viscosity of the energy storage layer and heat conduction coefficient of solid materials and the air, respectively; and $\lambda_m=(1-\varphi)\lambda_s+\varphi\lambda_a$,$\mu_m=\mu/\varphi$; K, C, respectively, represent permeability and inertia coefficient of the energy storage layer.

$$K=d_b{}^2\varphi^3/\left(175(1-\varphi)^2\right) \tag{11}$$

$$C=1.75\varphi^{-1.5}/\sqrt{175} \tag{12}$$

where d_b is the grain size of the porous medium.

2.3. Boundary conditions and solving procedures

The given boundary conditions are as follows: the heat transfer coefficient by convection between the collector canopy and the ambient is 10W/(m^2·K), with the ambient air temperature being 293K; the collector inlet serves as pressure entrance while the chimney outlet acts as pressure exit; the chimney wall is regarded as adiabatic; the given temperature of the energy storage layer bottom is 288K [32], where the soil temperatures several meters under the ground surface can be considered as constant and lower than the ambient. In addition, the solar radiation going all the way to the ground could be viewed as a heat source placed on a 0.1mm in a deep thin layer. Then the solar energy will be absorbed by this deep thin layer and

Int. J. Energy Res. 2013; **37**:310–322 © 2011 John Wiley & Sons, Ltd.
DOI: 10.1002/er

Table II. Boundary conditions.

Place	Type	Value
0.1 mm top layer of the ground	Heat source	2×10^6–10×10^6 W/m^3
Bottom of the ground	Temperature	288 K
Surface of the canopy	Wall	T=293 K; α=10 W/(m$^2\cdot$K)
Surface of the chimney	Wall	q_{chim}=0 W/m^2
Collector inlet	Pressure inlet	$P_{r,inlet}$=0 Pa; T_0=293 K
Chimney outlet	Pressure outlet	$P_{r,outlet}$=0 Pa
Turbine	Reverse fan	Pressure drop: 0–1000 Pa

changes into thermal energy. One part of this thermal energy will transfer to the airflow within the collector, the other part being stored within the energy storage layer and transferred to the deep ground. The gravitational acceleration is 9.8 m/s^2. Moreover, taking into consideration both the pressure distributions inside and outside the system, we define both the collector inlet and the chimney outlet as pressure boundaries and assume the relative pressures as 0 Pa, that is, the static pressures of same height inside and outside the collector inlet are the same, and those of same height inside and outside the chimney outlet are also the same. The air, therefore, flows through the chimney outlet without changing its velocity and maintains a constant dynamic energy [19]. The SC pressure-based turbine, though with nearly the same air velocity at its front and back, would not follow the Betz' theory in terms of output power due to the significantly changing pressures. Consequently, as to a given turbine pressure drop, the turbine output power could be obtained by Equation (13):

$$W_{shaft} = \eta_{shaft}\cdot\Delta p\cdot V \tag{13}$$

where, W_{shaft} is the turbine shaft output power; η_{shaft} is the turbine energy transfer efficiency: η_{shaft}=80%; Δp is the turbine pressure drop; V is the volume rate of flow of the air at the chimney outlet.

Table III. Comparison between the simulation results and the experimental data.

Solar radiation 1040 W/m^2	Experiment	Simulation	Error
Collector air ΔT (K)	25	25.26645	+1.066%
Ground surface T_{max} (K)	345	351.43248	+6.4 K
Output power (kW)	41	40.196	−1.96%
Chimney inlet velocity (m/s)	9	8.812802	−2.079%

For an SC system with an energy storage layer, solar radiation into the system can be divided to two parts: (i) energy absorbed by air flow inside the collector; and (ii) energy stored by the energy storage layer during daytime with solar radiation. The second part should not be included when we analyze the system efficiency. Thereby, the system efficiency can be obtained as follows:

$$\eta_{sys} = \frac{W_{shaft}}{Q_{air}} \tag{14}$$

where, η_{sym} is the system efficiency, and Q_{air} is the energy absorbed by the air flow inside the collector.

In the case of a three-dimensional numerical simulation, the whole configuration of the turbine can be given in detail without any assumptions like in this two-dimensional numerical simulation, and the turbine rotation speed can be given or controlled in advance [33].

According to Equation (13), there are two strategies to control the output power of the SCs: pressure drop across the turbine or volume flow rate [34]. These two parameters are coupled together in SC systems, one being confirmed if the other is given. As the volume flow rate is almost impossible to be known beforehand, the pressure drop across the turbine will serve as boundary condition in this numerical simulation. Detailed boundary conditions of different sections are shown in Table II.

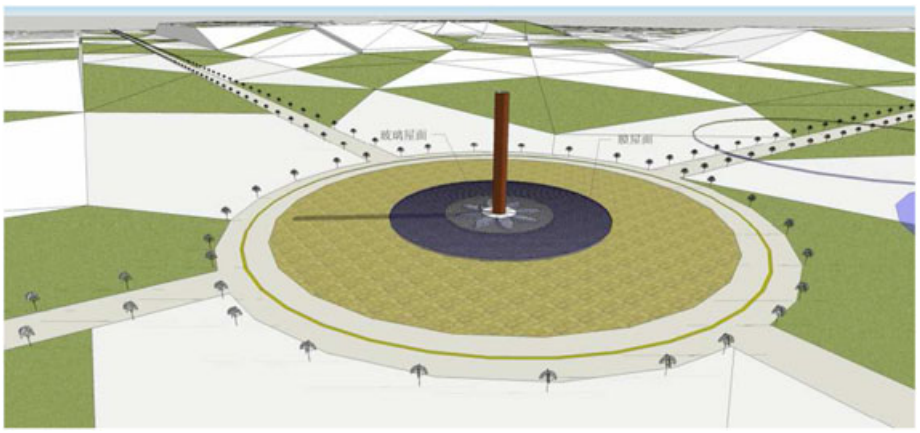

Figure 1. Sketch of a 10 MW solar chimney power generating system.

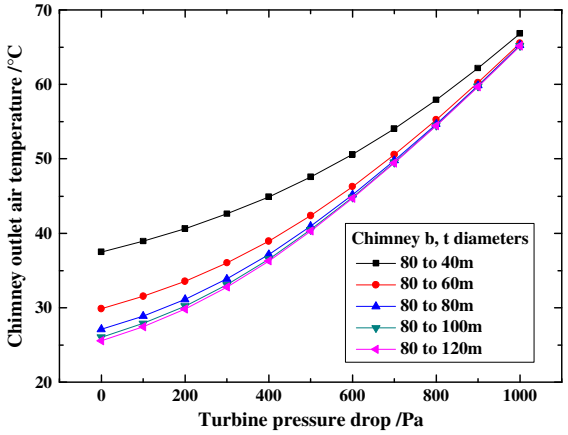

Figure 2. Comparison of chimney outlet air temperature.

The mesh number of the SC system was nearly 500,000. When numerical simulation procedure was executed, further increase in the mesh was less than 2% variation in the output power value which was taken as a criterion for grid independence. All the numerical simulations were carried out with the double precision solver. The iteration errors were 10^{-7} for continuity, momentum and turbulent equations, while it was 10^{-11} for the energy equation. The numerical simulation procedure was executed by using A standard PC with Intel Pentium Dual E2180 2.00GHz CPU and 4.00GB RAM, and the time spent for each simulation result was about 5–6 h. Cases of different chimney configuration had little effect on the time consumption of numerical simulation procedure.

3. VALIDITY

In order to verify the validity of the numerical simulation results in this paper, detailed comparison between the numerical simulation results and the experimental data collected was carried out. The computation parameters were set according to the following experimental data [3], which served as the boundary conditions and ambient conditions of the numerical program: solar radiation was 1040 W/m^2, ground absorptivity was 0.56–0.67, the transmissivity of the PVC membrane was 0.8, ambient temperature was 303 K, thermal conductivity of the soil from the surface to the deep ground was: 0–1 cm, 0.5 W/(m·K); 1–5 cm, 0.7 W/(m·K); 5–10 cm, 1.2 W/(m·K); 10–20 cm, 1.5 W/(m·K); 20–150 cm, 1.5 W/(m·K). Other detailed experimental data and the corresponding numerical simulation results are shown in Table III. As indicated in Table III, the simulation results are quite consistent with the experimental data. Besides, its difference from the experimental data is less than 2.5%. These errors may be ascribed to the following parameters which were not reported in literature [3]: ambient air velocity, cloud in the sky, ground absorptivity and the PVC transmissivity distributions along the collector radius and the ambient air humidity. Hence, it can be concluded that the numerical simulation method applied in this paper is effective and feasible.

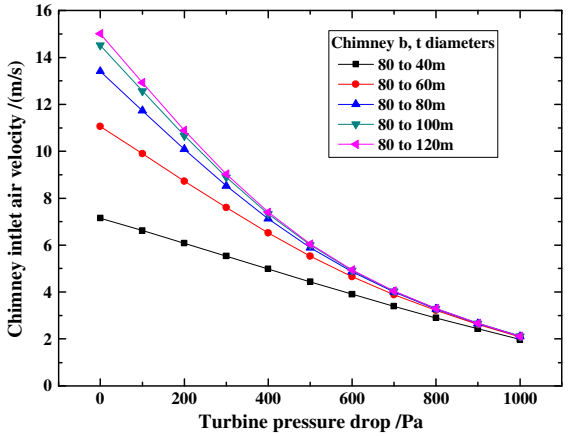

Figure 3. The effect of chimney shape and turbine pressure drop on chimney inlet air velocity.

Int. J. Energy Res. 2013; **37**:310–322 © 2011 John Wiley & Sons, Ltd.
DOI: 10.1002/er

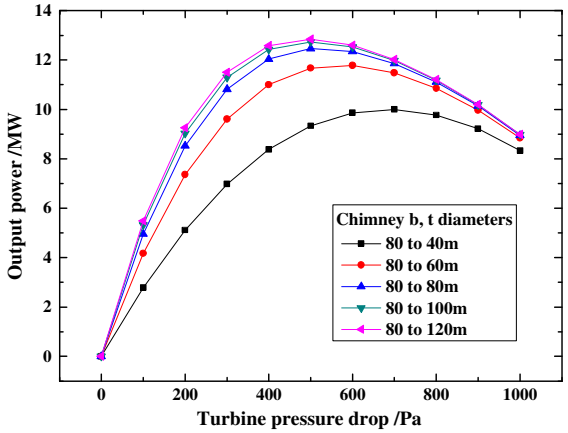

Figure 4. The effect of chimney shape and turbine pressure drop on system output power.

4. RESULTS AND ANALYSIS

When the solar radiation is absorbed by the energy storage layer, the temperature of the energy storage layer will increase, with solar energy being stored as thermal energy. This stored thermal energy will be divided into three parts, one part is used to heat the air inside the collector, part of which will ultimately transform to electricity; one part is stored for the system night-running, leaving the rest transferring to the deep underground as heat loss. Detailed description can also be seen in related references [3,6] (Figure 1).

4.1. Comparison based on equal chimney bottom section area

As shown in Table I, Case 1 mainly focuses on how the chimney configuration affects system performance parameters under the circumstances of equal chimney bottom section area. With the bottom diameter remaining 80m, five cases, namely, the chimney top diameter being 40m, 60m, 80m, 100m and 120m respectively, are to be analyzed. Among them, the first two are conical chimneys, while the last two are divergent ones. Top diameter being 40m or 120m, the field angle of an 800m-high chimney is 2.86°, which is still within our capacity. With the solar radiation energy being 500W/m^2 and the ambient temperature being 293K, the calculations are carried out, whose results are shown in Figure 2 to Figure 5.

The driving force of a SC comes from the difference between air density of the outside air and the air inside the chimney, which will be enlarged with the increase of chimney height. For a certain SC being given collector and chimney geometric parameters, the volume flow rate and air temperature increase can be obtained if boundary conditions are given as shown in Table II. Maximum volume flow rate, minimum air temperature increase and buoyancy are obtained if the pressure drop across the turbine is set at 0 Pa. An increase of turbine pressure drop will result in a higher air temperature, greater buoyancy and lower flow rate.

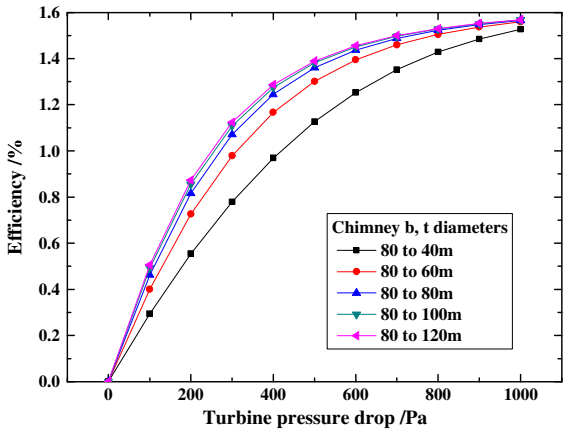

Figure 5. The effect of chimney shape and turbine pressure drop on system efficiency.

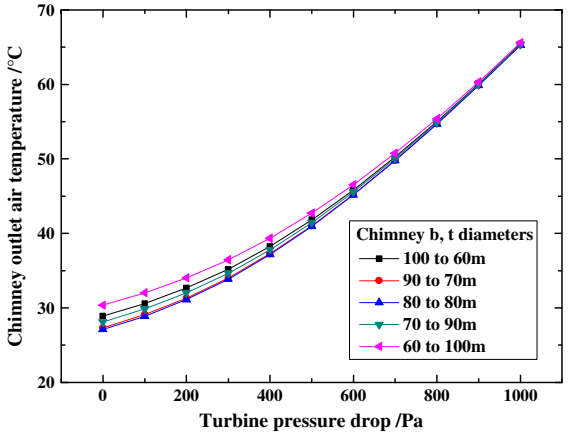

Figure 6. The effect of chimney shape and turbine pressure drop on chimney outlet air temperature.

It is clear that chimney configurations also have an effect on the thermal performance of SCs. The impacts of chimney configurations on its outlet air temperature and inlet air velocity are respectively illustrated in Figure 2 and Figure 3. It can be seen that with the growth of turbine pressure drop, the outlet air temperature climbs while the inlet air velocity slowly decreases, since growing pressure drop lessens the air flow driving force and velocity, thus increasing the air temperature. Besides, based on a given pressure drop, the outlet air temperature lowers and the inlet air velocity goes up as the top diameter of the chimney increases, but the variation becomes insignificant when the diameter is larger than 80m. Pressure drop being above 800Pa, cylindrical and divergent chimneys are nearly the same in outlet air temperature and inlet air velocity.

The influences of different chimney configurations on system output power and efficiency are demonstrated in Figure 4 and Figure 5. It could be seen from Figure 4 that, when the chimney top diameter remains unchanged, the output power first goes up before going down with an increasing turbine pressure drop, and it is positively correlated with the diameter variation of the chimney top based on a given pressure drop. When the diameter is less than 80m, its growth brings about obvious increment in output power which changes insignificantly as the diameter is larger than 80m. We may come to the conclusion that it is unwise to choose the conical chimney for its relatively smaller output power. In addition, it is worth mentioning that a larger diameter lessens the pressure drop needed for driving the output power to hit its peak value. While an insignificant decrease in air flow velocity caused by the increase of a relatively small turbine pressure drop raises the production of the volume rate of air flow and the pressure drop, a bigger turbine pressure drop would greatly influence the air velocity, thus lowering the output power.

Figure 5 shows that when the chimney top diameter remains a constant, the system efficiency rises with the increasing turbine pressure drop, and when the turbine pressure drop is given, it goes up with the increasing diameter as well. Just the same as the output power, as the diameter is larger than 80m, the efficiency varies insignificantly

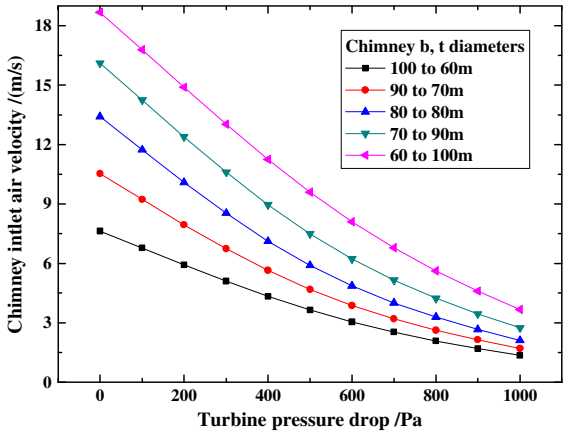

Figure 7. The effect of chimney shape and turbine pressure drop on chimney inlet air velocity.

Int. J. Energy Res. 2013; **37**:310–322 © 2011 John Wiley & Sons, Ltd.
DOI: 10.1002/er

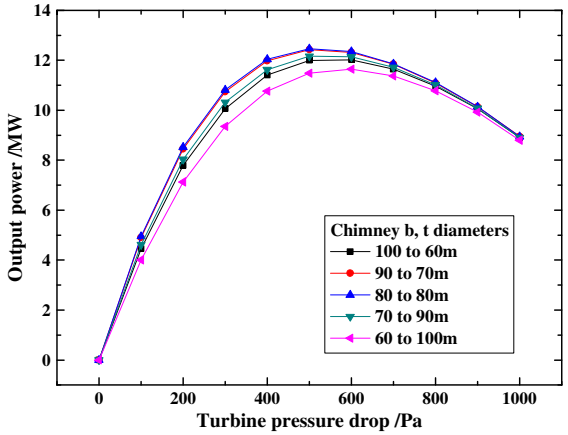

Figure 8. The effect of chimney shape and turbine pressure drop on system output power.

with the change of chimney top diameter. In terms of the SC system, the divergent chimney will lead to a significant increase in costs with only a small increment in system output power and efficiency as shown in Figure 4 and Figure 5. Therefore, it is proved to be unnecessary.

4.2. Comparison based on equal chimney surface area

As shown in Table I, Case 2 mainly analyzes, assuming equal chimney surface area, how different chimney configurations influence system performance parameters. The chimneys' average diameter remains 80 m. Choosing five types of chimneys whose diameter variation spans from bottom to top are 100–60 m, 90–70 m, 80–80 m, 70–90 m and 60–100 m; the calculations are conducted with the solar radiation energy being 500 W/m^2 and the ambient temperature being 293 K, whose results are shown in Figure 6 to Figure 9. The comparisons are made between chimneys of the same chimney surface area, as the costs of the chimneys are in proportion to their chimney surface area [3,11]. It follows that the divergent chimney may cost more than the conical one, and it would be appropriate to choose the former one if its output power and efficiency could be improved.

The effects of the chimney top diameter and turbine pressure drop on the chimney outlet air temperature and inlet air velocity are shown in Figure 6 and Figure 7. As mentioned before, as turbine pressure drop increases, the outlet air temperature climbs while the inlet air velocity gradually falls. Besides this, for a given turbine pressure drop, the outlet air temperature of the cylindrical chimney is the lowest while the inlet air velocity decreases as the chimney bottom diameter becomes larger. Figure 8 and Figure 9 respectively describe the impact of chimney configuration and turbine pressure drop on system output power and efficiency. It could be seen that, in terms of system output power and efficiency, the cylindrical chimney would be the best choice among all the three, as it has the smallest total flow resistance and the largest mass flow

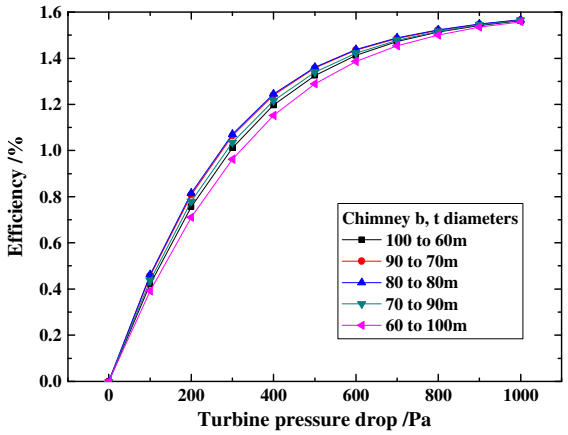

Figure 9. The effect of chimney shape and turbine pressure drop on system efficiency.

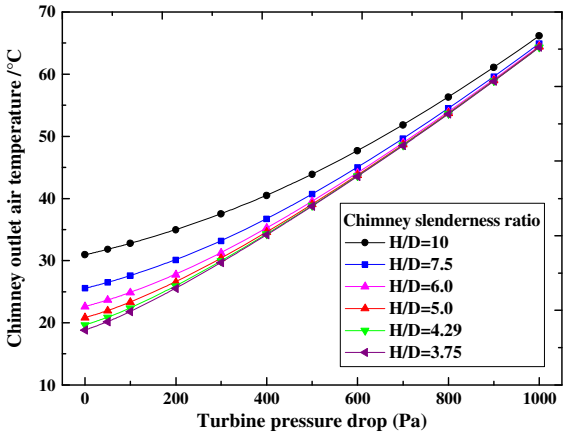

Figure 10. The effect of chimney slenderness ratio on chimney outlet air temperature.

rate, thus reaching the optimum value of output power and efficiency. To conclude, it would be best to use cylindrical chimney in the SC system.

4.3. The influence of the chimney slenderness ratio, H/D

In order to determine the details of the chimney configuration, the influence of H/D of the chimney is analyzed in this part. As shown in Case 3 of Table I, comparisons were made between cylindrical chimneys of different H/Ds by changing their diameters (60m–160m). The calculations were carried out with the solar radiation energy being 600W/ m^2 and the ambient temperature being 293K, and the results are shown in Figure 10 to Figure 13.

Figure 10 and Figure 11 illustrate how the chimney diameter and turbine pressure drop affect the chimney outlet air temperature and chimney inlet air velocity, showing the chimney diameter remaining a constant. The chimney outlet air temperature continuously increases while the inlet air velocity takes on a reverse changing trend as the turbine pressure drop grows. As for an invariable turbine pressure drop, a longer chimney diameter (a smaller H/D) gives rise to a lower outlet air temperature and a smaller inlet air velocity. However, the decreases of the temperature and velocity gradually slow down and become really unnoticeable until the diameter reaches 120m.

Figure 12 and Figure 13 describe how chimney diameter and turbine pressure drop affect the system output power and efficiency, illustrating that the chimney diameter's growth within 100m brings about a noticeable increment in output power and efficiency while its rise only leads to tiny change in output power and efficiency when it is beyond 100m. Therefore, we can see from these two figures that it would be best to use chimney with H/D within 6–8 in the SC system. The chimney would be 120–170m in diameter if it is 1000m high, which is fully consistent with Schlaich's design [6], and also with Petrorius findings [35] that the optimum slenderness ratio in terms of output power is around 5 or 6, smaller H/D increasing the risk for the plant to experience cold air inflow.

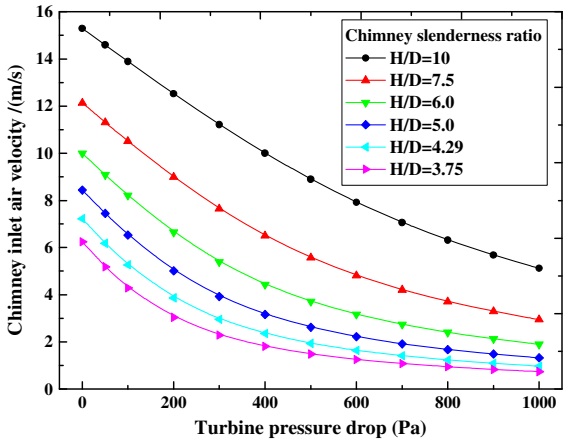

Figure 11. The effect of chimney slenderness ratio on chimney inlet air velocity.

Int. J. Energy Res. 2013; **37**:310–322 © 2011 John Wiley & Sons, Ltd.
DOI: 10.1002/er

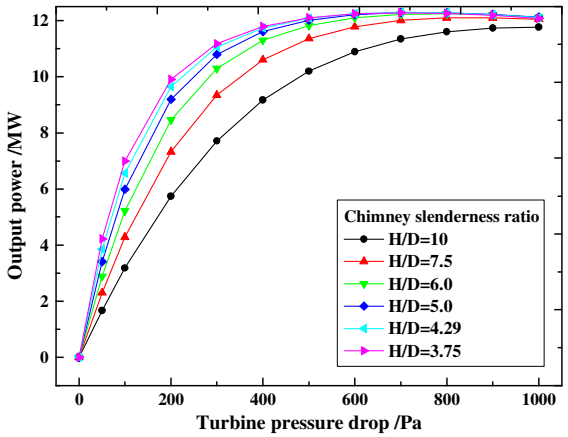

Figure 12. Comparison of system output power.

It should be pointed out that, comparing Figure 12 with Figures 4 and 8, the variation of output power with turbine pressure drop is not in the same way. This is because the combination of collector radius and chimney height can affect the total pressure potential of the system. Higher chimney can result in larger driving force, but less collector area will not make the air temperature increase to a certain value with a given solar radiation, so the system output power decreases rapidly when the turbine pressure drop increase to some extent.

The following analysis will concentrate on the effect of the chimney slenderness ratio H/D and solar radiation on system performance. With the geometric parameters shown in Case 3 of Table I, we carried out a study on the corresponding variation of performance parameters when global solar radiation changes from 200 W/m^2 to 1000 W/m^2. The influence of chimney H/D and solar radiation on system output power and efficiency could be worked out (as shown in Figure 14 and Figure 15), with the turbine pressure drop remaining 400 Pa. From these figures, it can be seen that output power increases and system efficiency decreases with increasing solar radiation, the reason of which can be found in former research work [18,20]. Furthermore, the figures also show that, when the chimney diameter is within 100 m (H/D > 6), the output power and efficiency increase significantly as the diameter rises, but they change insignificantly with a diameter beyond 100 m. This further increase in diameter would only lead to a higher cost. Therefore, on the premise of a comprehensive consideration of the chimney construction costs, an optimized chimney diameter for a certain chimney height can be achieved according to the above results.

5. CONCLUSION

The chimney is a key part in providing driving force for the SC system, and an appropriate configuration design would in a way lower the total system construction costs. The steady state numerical simulation

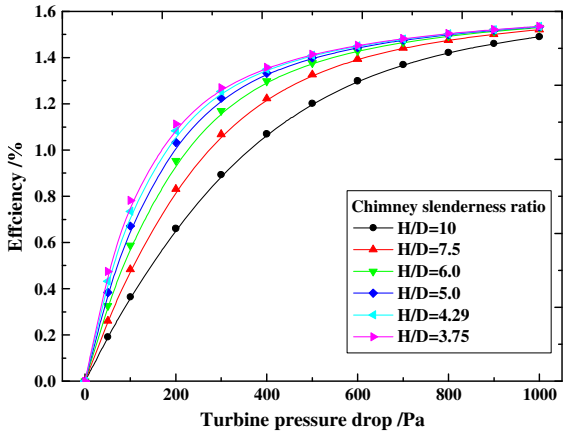

Figure 13. The effect of chimney slenderness ratio on system efficiency.

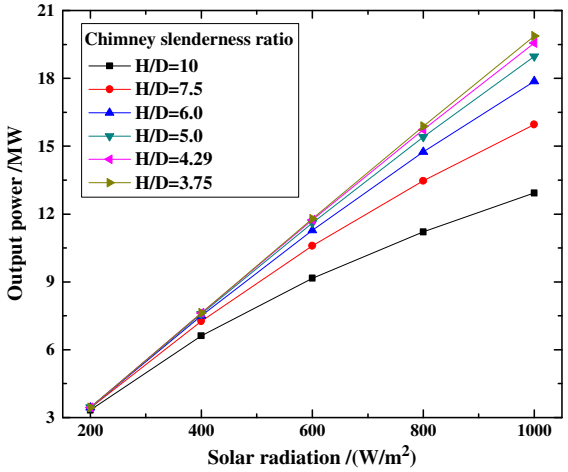

Figure 14. The effect of chimney slenderness ratio and solar radiation on system output power.

based on two-dimensional assumptions is carried out in this paper, with the intention of analyzing how chimney configuration influences the SC system characteristic parameters such as output power and efficiency, the steady state numerical simulation based on two-dimensional assumptions is carried out in this paper. According to the numerical simulation results, both the divergent chimney and the conical chimney are not recommended to be used in the system. The former one, though to some degree improves the system efficiency and output power, also causes increases in construction costs as well, and for the conical one, both the efficiency and output power decrease greatly. Therefore, after an overall analysis of the configuration's influence on system output power and efficiency, it would be best to use the cylindrical chimney, whose optimum H/D value could be chosen from 6 to 8 in actual construction.

NOMENCLATURE

D = Chimney diameter (m)
u = Average velocity magnitude in the axial direction (m/s)
r = Co-ordinate in radial direction (m)
T = Temperature (K)
T_0 = Temperature of the environment (K)
g = Gravity, g=9.807 (m/s^2)
Pr = Prandtl number (dimensionless),Pr $= \frac{c_p \mu}{k}$
X = Co-ordinate in axial direction (m)
S_ϕ = Source item

Greek symbols

Δ = Difference or increase
v = Kinematic viscosity (m^2/s)
μ_t = Turbulent dynamic viscosity coefficient

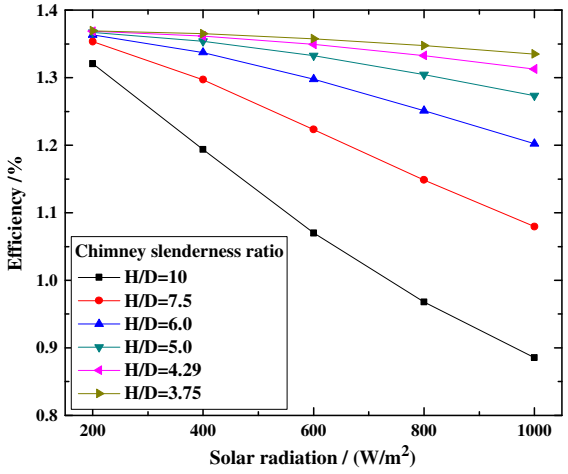

Figure 15. The effect of chimney slenderness ratio and solar radiation on system efficiency.

Int. J. Energy Res. 2013; **37**:310–322 © 2011 John Wiley & Sons, Ltd.
DOI: 10.1002/er

μ = Dynamic viscosity (kg/(m·s))
β = Coefficient of cubic expansion
ρ = Density (kg/m^3)
κ = Turbulent kinetic energy (J/kg)
ε = Dissipation (W/kg)
σ_ε = Prandtl number of dissipation
σ_T = Prandtl number of turbulence
σ_κ = Prandtl number of pulse kinetic energy 1.0
Γ_ϕ = Generalized diffusion coefficient

Subscript

b = Chimney bottom
e = Environment
t = Viscous dissipation effect caused by turbulent characteristics
ε = Dissipation
κ = Kinetic energy
ϕ = Porosity
t = Chimney top
T = Turbulent flow

ACKNOWLEDGEMENT

This work was supported by the National Key R&D Program of China (Grant No. G2007CB206903) and the National Natural Science Foundation of China (Grant No. 51036003, 50721005).

REFERENCES

1. http://www.gov.cn/english/2010-03/05/content_1548250.htm.
2. Haaf H, Friedrich K, Mayer G, *et al*. Solar chimneys, Part a. *International Journal of Solar Energy* 1983; **2**(1):3–20.
3. Haaf H. Solar chimneys, Part b. *International Journal of Solar Energy* 1984; **3**(2):141–161.
4. Weinrebe G. Greenhouse gas mitigation with solar thermal powerplants. Proceedings of the PowerGen Europe 1999 Conference, Frankfurt, Germany, 1–3 June 1999.
5. Bernardes MADS. Life Cycle Assessment of Solar Chimneys, World Renewable Energy congress VIII. Proceedings of the World Renewable Energy congress VIII, Denver, USA, 2004.
6. Schlaich J, Bergermann R, Schiel W, *et al*. Design of commercial solar updraft tower systems-utilization of solar induced convective flows for power generation. *ASME Journal of Solar Energy Engineering* 2005; **127**(1):117–124.
7. Gannon AJ, von Backström TW. Solar chimney cycle analysis with system loss and solar collector performance. *Journal of Solar Energy Engineering* 2000; **122**(3):133–137.
8. Pretorius JP, Kröger DG. Critical evaluation of solar chimney power plant performance. *Solar Energy* 2006; **80**(5):535–544.
9. Ming TZ, Zheng Y, Liu C, *et al*. Simple analysis on thermal performance of solar chimney power generation systems. *Journal of Energy Institute* 2010; **83**(1): 6–11.
10. Pasumarthi N, Sherif SA. Experimental and theoretical performance of a demonstration solar chimney model-part: mathematical model development. *International Journal of Energy Research* 1998; **22**(3): 277–288.
11. Pasumarthi N, Sherif SA. Experimental and theoretical performance of a demonstration solar chimney model-part II: experimental and theoretical results and economic analysis. *International Journal of Energy Research* 1998; **22**(5):443–461.
12. Padki MM, Sherif SA. On a simple analytical model for solar chimneys. *International Journal of Energy Research* 1999; **23**(4):345–349.
13. von Backström TW, Fluri TP. Maximum fluid power condition in solar chimney power plants-an analytical approach. *Solar Energy* 2006; **80**(11):1417–1423.
14. Kirstein CF, von Backström TW. Flow through a solar chimney power plant collector-to-chimney transition section. *Journal of Solar Energy Engineering* 2006; **128**(3):312–317.
15. Pastohr H, Kornadt O, Gurlebeck K. Numerical and analytical calculations of the temperature and flow field in the upwind power plant. *International Journal of Energy Research* 2004; **28**(6):495–510.
16. Maia CB, Ferreira AG, Valle RM, *et al*. Theoretical evaluation of the influence of geometric parameters and materials on the behaviour of the airflow in a solar chimney. *Computers & Fluids* 2009; **38**:625–636.
17. Bonnelle D, Siros F, Philibert C. Concentrating solar parks with tall chimneys dry cooling. Solar paces International conference, Perpignan, France, September 2010.
18. Ming TZ, Liu W, Xu GL. Analytical and numerical simulation of the solar chimney power plant systems. *International Journal of Energy Research* 2006; **30**(11):861–873.
19. Ming TZ, Liu W, Pan Y, *et al*. Numerical analysis of flow and heat transfer characteristics in solar chimney power plants with energy storage layer. *Energy Conversion and Management* 2008; **49**(10):2872–2879.
20. Xu GL, Ming TZ, Pan Y, *et al*. Numerical analysis on the performance of solar chimney power plant system. *Energy Conversion and Management* 2011; **52**(2): 876–883.

21. Zheng Y, Ming TZ, Zhou Z, *et al*. Unsteady numerical simulation of solar chimney power plant system with energy storage layer. *Journal of the Energy Institute* 2010; **83**(2):86–92.
22. Ninic N. Available energy of the air in solar chimneys and the possibility of its ground-level concentration. *Solar Energy* 2006; **80**(7):804–811.
23. Zhou XP, Yang JK, Xiao B, Shi XY. Special Climate around a Commercial Solar Chimney Power Plant. *Journal of Energy Engineering* 2008; **134**(1):6–15.
24. van Reken TM, Nenes A. Cloud Formation in the Plumes of Solar Chimney Power Generation Facilities: A Modeling Study. *Jounal of Solar Energy Engineering* 2009; **131**(1):011009.
25. Zhou XP, Yang JK, Ochieng RM, Li XM, Xiao B. Numerical investigation of a plume from a power generating solar chimney in an atmospheric cross flow. *Atmospheric Research* 2009; **91**(1):26–35.
26. Lang C, Altmever F, Weigl J. Earthquake Behavior of Large Hyperbolical Shells - From Natural Draft Cooling Towers to Solar Power Plant Chimneys. 2d International Conference on Solar Chimney Power Technology, 7p in CD-Proceedings, Ruhr-University Bochum, Germany, September 2010.
27. Krätzig WB, Harte R, Montag U, Wörmann R. *From large natural draught cooling towers to chimneys of solar updraft power plants. 16p*. In *Evolution and Trends in Design, Analysis and Construction of Shell and Spatial Structures, IASS Symposium 2009, CD-Proceedings*. Domingo A, Lazaros C (eds.). TU Valencia, Spain, 2009.
28. Harte R, Krätzig WB, Niemann H-J. From Cooling Towers to Chimneys of Solar Upwind Power Plants. 10p in Proceedings of 2009 Structures Congress, Austin, Texas, 2009.
29. Serag-Eldin MA. Computing Flow in a Solar Chimney Plant Subject to Atmospheric- Winds. Proceedings of HTFED04, ASME Heat Transfer /Fluids Engineering Summer Conference, Charlotte, N.C., July 11–15, 2004, paper No. HT-FED2004-56651.
30. Serag-Eldin MA. Mitigating Adverse Wind Effects on Flow In Solar Chimney Plants. Proceedings of the 4th International Engineering Conference, Sharm El-Sheikh, April 20–22, 2004, paper No.318.
31. Sung JK. Convective heat transfer in porous and overlying fluid layers heated from below. *International Journal of Heat and Mass Transfer* 1996; **39**(2): 319–329.
32. Fan AW. Theoretical and Experimental Investigation on Thermophysical Problems in Resources-Environment-Plant system. Chapter 3: Numerical simulation on the soil temperature in various conditions. PhD thesis Huazhong University of Science and Technology, 2004; 20–32.
33. Ming TZ, Liu W, Xu GL, Xiong YB, Guan XH, Pan Y. Numerical simulation of the solar chimney power plant systems coupled with turbine. *Renewable Energy* 2008; **33**(5):897–905.
34. dos Santos Bernardes MA, von Backstrom TW. Evaluation of operation control strategies applicable to solar chimney power plants. *Solar Energy* 2010; **84**(2): 277–288.
35. Pretorius JP. Optimization and control of a large-scale solar chimney power plant. Chapter 4: Thermo-economic plant optimization, PhD thesis University of Stellenbosch, 2007; 55–67.